DOI: https://doi.org/10.1016/j.apsusc.2015.11.253

ACCEPTED VERSION

Silver and Gold Nanoparticles produced by Pulsed Laser Ablation in Liquid to investigate their interaction with Ubiquitin

M. Dell'Aglio[a], V. Mangini[b], G. Valenza[a,b], O. De Pascale[a], A. De Stradis[c], G. Natile[b], F. Arnesano[b], A. De Giacomo[a,b]

[a] CNR-NANOTEC, Via Amendola 122/D, 70126, Bari, Italy

[b] Department of Chemistry, University of Bari "Aldo Moro", Via Orabona 4, Bari, Italy

[c] CNR-IPSP, UOS Bari, Via Amendola 165°, 70126, Bari, Italy

Abstract

The interaction of nanoparticles (NPs) with proteins is widely investigated since it can be a key issue in addressing the problem of nanotoxicity, in particular for biological and medical applications. Therefore, silver and gold nanoparticles (AgNPs and AuNPs) were produced in water by Pulsed Laser Ablation in Liquid (PLAL) and allowed to react with Ubiquitin (Ub), (a small human protein essential for degradative processes in cells). NPs produced by PLAL are completely free of undesired contaminants and do not require the use of stabilizers. We found that the NPs+Ub system behaves differently if the NPs are or are not treated with stabilizer before performing the interaction with Ub, since the presence of capped agents modify the surface reactivity of the metal-NPs. The surface plasmon resonance (SPR) absorption spectroscopy has been employed to monitor the fast changes occurring in the NP colloidal solutions upon interaction with Ub. The SPR results were confirmed by TEM analysis. It is found that when Ub interacts with naked NPs a rapid aggregation occurs and, at the same time, Ub undergoes an amyloid transition. In particular the aggregation of AuNPs occurs at a much greater rate than that of analogous AgNPs.

Keywords: Silver nanoparticles, Gold nanoparticles, laser ablation in liquids, Ubiquitin, nanoparticles-protein interaction, Amyloid-like aggregation.

1. Introduction

In the last decade the synthesis of nanoparticles (NPs) by Pulsed Laser Ablation in Liquid (PLAL) has gained wide interest thanks to the possibility to produce NPs completely free of undesired contaminants, to avoid the use of harmful reactants, and to accomplish long-lasting stability without using any stabilizer [1,2]. The stabilizer can affect deeply the chemical reactivity of the NPs surface and its role has to be taken into account when planning biological and medical applications. The peculiarity of the NPs produced by PLAL lies in the particular environment in which they are produced [3,4]: the plasma induced by the laser on a target submerged in water, as well as the subsequent cavitation bubble formation and dynamics, play crucial roles in the NPs formation mechanisms and stability.

The interaction of NPs with proteins has extensively been studied for medical and biological applications [5], since it is known that, once the NPs entered in the biological fluids, a rapid interaction of NPs with plasma proteins takes place. Adsorbed proteins form the so-called protein corona around the NPs [6]. The structure and the normal protein function can be modified, thus leading to unexpected biological reactions [7]. The NPs surface plays a crucial role in the process of corona formation and, if a stabilizer is present in the solution, the surface reactivity can change dramatically. Usually, protein-NPs investigations are carried out with NPs coated with a stabilizer, so that the protein corona formation can be different from that of naked NPs. Recently, some studies [8, 9] have started to address this issue by investigating the interaction of different proteins with naked NPs. For instance, AuNPs [10] and AgNPs [11] produced by PLAL were mixed with bovine serum albumin (BSA) showing the classical protein corona formation. However, in a previous work from our laboratories [12], we demonstrated how naked AgNPs interact with Ubiquitin (Ub) differently from stabilized AgNPs. Thus, while colloidal solutions of citrate-stabilized AgNPs react with Ub forming a protein corona which is stable over time [12,13], the interaction of naked AgNPs with Ub leads to a protein corona followed by rapid aggregation of the NPs, simultaneously with an amyloid transition of the protein which appears to be responsible for NP clustering

Ub is a human protein with important biological functions (e.g., it flags proteins for degradation by the proteasome). Its relatively small size and well-characterized three-dimensional structure make it a good model for investigating the interaction between proteins and NPs.

In this work, we performed similar interaction experiments with AgNPs or AuNPs produced by PLAL, in order to understand if naked NPs of different metals can aggregate as a consequence of interaction with Ub and amyloid transition of the protein.

Moreover, since plaques and inclusions composed of fibrillar deposits of Amyloid β (Aβ) and other proteins are the hallmark of several neurodegenerative disorders, the study of amyloid-like aggregation has become relevant in the biological and medical field.

AgNPs and AuNPs were produced in pure water and, after selecting the best experimental conditions for PLAL, the produced NPs were characterized and allowed to react with Ub while we monitored the intervening changes as a function of time. The interaction between NPs and Ub were performed in the presence or absence of stabilizer, in order to test the NPs surface reactivity. Finally, the system "AuNPs+Ub" was tested to demonstrate that also with naked AuNPs the Ub reveals an amyloid transition. So a preincubation of AuNPs solution with transthyretin (an inhibitor of amyloid-type aggregation) before the treatment with Ub, an incubation of AuNPs with a Ub mutant (E16V) and finally a thioflavin T assay (indicative of the amyloid form of protein) on "AuNPs+Ub" aggregate have been employed.

2. Experimental set-up

The experimental setup for the production of NPs in water has been extensively described in previous works [12,14]. It consists of nanoseconds Nd-YAG lasers (Quanta System PILS-GIANT and Quanta System Thunder) operating both with fundamental and second harmonic generation (1064 nm and 532 nm, respectively), having a laser frequency of 10 Hz and a nominal pulse duration of 8 ns. Depending upon the experiment, different laser wavelengths (1064 and 532 nm) were used and different lens were employed to focus the laser on a metal target submerged in water. All colloidal solutions were produced in ultrapure Milli-Q water.

Soon after production, colloidal solutions were monitored as a function of time by surface plasmon resonance (SPR) absorption spectroscopy using an Ocean Optics (USB2000+XR) spectrometer with a light source (Mini Deuterium Halogen Light Source DT-Mini-2-GS**)**. The transmission electron microscopy (TEM) analysis was performed using a Philips Morgagni 282D TEM, operating at 60 kV

Fluorescence imaging of the samples was performed by means of Laser Scanning Confocal Microscopy (LSCM) using the TCS SP8 SMD confocal microscope by LEICA equipped with a white a blue diode laser (excitation wavelength was 405 nm). Samples were observed through a 20x dry objective and the emission in the range 420-600 nm was collected by a hybrid detector; at the same time the transmitted light was independently collected by a conventional PMT detector.

3. Materials and methods

The best experimental conditions for NP production by PLAL were chosen on the basis of reproducibility, size distribution, and stability in time. After the production by PLAL, the NPs were monitored for at least two days with SPR absorption spectroscopy, this time being sufficient for the NPs to reach the equilibrium.

For the production of AgNPs in water a 532 nm NdYAG (Quanta System PILS-GIANT) laser was focused on a silver target immersed in a cuvette filled with 3 ml of water by using 4 cm focal lens, irradiance of 17 GW/cm^2**,** and laser ablation time of 3 min. The silver target was purchased from Goodfellow Cambridge Limited.

For the production of AuNPs in water a 1064 nm NdYAG (Quanta System Thunder) laser was focused on a gold target immersed in a vessel filled with 25 ml of water by using of a 5 cm focal lens, irradiance of 71 GW/cm^2, and a laser-ablation time of 10 min. The gold target was purchased from Kurt J. Lesker Company.

The molar concentrations (mols of NPs/liter) of the NPs solution were calculated by applying the Lambert-Beer law to the absorbance spectra of the colloidal solutions. The extinction coefficients, which depend upon the NPs size, were measured via appropriate calibration curves for AgNPs and AuNPs. The standard solutions used for calibration were: AgNPs of 10 nm particle size in 2 mM citrate purchased from Nanocomposix (10 nm Citrate NanoXact^{TM} Silver, 0.022 gL^{-1}); AuNPs of 10, 20, 40, 60, 80 and 100 nm particle size in 2 mM citrate purchased from Sigma Aldrich (ranging from 0.06 gL^{-1} to 0.04 gL^{-1}). The concentrations of NPs solution used in this work were 2.2 and 2.4 nM for AgNPs and AuNPs, respectively.

The NPs size was determined by TEM and SPR absorption spectroscopy and resulted to be 10 ± 3 and 15 ± 4 nm for AgNPs and AuNPs, respectively.

The incubation of NPs with wild-type Ub and the Ub mutant Glu16Val (E16V) was performed by dissolving the lyophilized protein in ultrapure water and adding an aliquot to the NP solution to obtain a final protein concentration of 25 μM. Ub was always added to the NP solution after 2 days from PLAL preparation. Wild-type Ub and E16V used in this work has been prepared as described in ref [12].

The sample treatment for TEM analysis (sample deposition on a grid with or without negative staining) as well as the sample preparation for the thioflavin T (ThT) assay have already been described (ref. [12]).

The whole set of colloidal solutions incubated with wild-type Ub (or with E16V, or preincubated with transthyretin (TTR)) was monitored as a function of time by SPR absorption spectroscopy.

4. Production and characterization of silver and gold nanoparticles

4.1 Pulsed Laser Ablation in Liquid

To produce NPs a laser pulse is focused on a target immersed in a liquid (pure water in our experiments). If the laser irradiance overcomes the breakdown threshold (so to induce a breakdown of the material) a plasma is generated. Once the plasma is formed it expands supersonically driving a shockwave and then extinguishes in several hundreds of nanosecond. Usually, the laser-induced plasma is characterized by high excitation temperature (≈10000-6000 K) and high electron density (≈10^{17} cm^{-3}). The plasma energy is rapidly transferred to the surrounding liquid, thus inducing a vaporization at the front head of the plasma itself, which leads to the formation of a cavitation bubble. In these conditions the plasma is subjected to a strong confinement effect, and consequently a fast plasma cooling occurs with a strong increase of the rate of the recombination phenomena (the total amount of emitting species decreases because atoms aggregate to generate the NPs and are subtracted from the collisional plasma [3]). The ablated material can condense in small NPs that are transferred to the cavitation bubble. The subsequent cavitation bubble dynamics consists of an expansion and a shrinking phase with a lifetime of hundreds of microseconds (one order of magnitude bigger than the plasma lifetime). The extreme conditions of temperature and pressure [15] reached in the plasma are believed to be responsible for the formation of NPs, while the bubble dynamics is connected to the release of the NPs and their stabilization in solution [3].

The NPs produced by PLAL, have prevalently spherical shape, particularly the metallic ones (Ag, Au, Cu), as widely reported in the literature [2,10]. The surface of these NPs results to be negative, as confirmed by ζ potential measurements (ζ values comprised between -30 and -45 mV). Recent studies on stability of NPs produced by PLAL focalize on the comprehension of surface features of this type of NPs [16,17].

4.2 Monitoring of metal nanoparticle in solution by surface plasmon resonance absorption spectroscopy

The first fast screening of the NP solution was performed via SPR absorption spectroscopy, which can be used to gain direct information on metal NPs in solution and also to monitor their interactions with proteins [11, 12].

The absorption spectra of colloidal solutions of metal NPs exhibit typical absorption bands in the UV-vis region [18] that provide information on the size, structure and aggregation properties [19]. In the case of spherical AgNPs and AuNPs, absorption spectra have been widely investigated both experimentally and theoretically [20]. It was found that the resonance wavelength of the SPR peak (here named λ_{SPR}) is related to the size of the NPs [20], but the relation between λ_{SPR} and size differs for NPs smaller than 25 nm for which the Mie theory is no more applicable. For instance for AuNPs it was found [21] that the size can be correlated to the ratio of absorbance at λ_{SPR} and that at 450 nm. The above correlation is valid as long as the NPs can be considered of spherical shape, as is the case of metal NPs produced by laser ablation [10], and when no clustering of NPs is present in solution. Moreover, the absorbance obeys the Lambert Beer law when the scattering contribution to the total extinction can be neglected, as in the case of NPs smaller than 30 nm [22] (such as those produced in these experiments). To estimate the NP concentration from SPR band, the extinction coefficient has to be accurately determined for each specific NP type and each NP size. The changes in size distribution (i.e. in the time following the production), can be qualitatively monitored by analysis of the absorbance bandwidth, that is related to the particle size distribution when the NPs are spherical [23].

4.3 Silver Nanoparticles in water

NPs suitable for studying their reactivity with Ub, were obtained by irradiation of a silver target directly in pure water.

To find the best experimental parameters for the production of AgNPs, the SPR absorption spectra were acquired during the laser ablation with the aim of monitoring the quality of the produced AgNPs. The optimum laser ablation time was then chosen in order to obtain the highest possible concentration with the highest reproducible size of AgNPs. It is important to underline that increasing the laser ablation time improves the fragmentation [24] and increases the concentration. At the same time, if the concentration of the colloidal solution increases over a certain value, the

Debye length decreases [25] together with the repulsive forces between the NPs, thus increasing the probability that NPs enlarge their size and form clusters or aggregates.

Therefore, the laser ablation time chosen for the experiments reported in this work was 3 min, since it allows to produce AgNPs stable for long time, as shown in Figure 1, where the wavelength, the absorbance and the width of the SPR band have been monitored as a function of time after laser ablation. Once the AgNPs are produced, they reach a thermodynamic equilibrium in solution in 24 h time and then remain stable for long time, although some negligible changes can be observed over some weeks. In particular, the wavelength and the width of the SPR band tend to increase while the absorbance decreases, probably because of deposition of NPs on the vessel walls. For these reasons, the reaction of AgNPs with Ub was generally performed 2 days after their production.

Figure 4 reports the absorbance spectrum of the AgNPs used in this work together with TEM analysis. The absorbance band indicates that the particle shape is nearly spherical (as confirmed by TEM images) since there are no blue or red shifted shoulders on the SPR band. The average size of AgNPs is 10.6 ± 2.6 nm, as measured by TEM image using ImageJ software. To calculate the AgNPs concentration, a calibration curve was drawn by using silver colloidal standard solutions of known concentration and particle size distribution. By plotting the absorbance of the SPR peak as a function of concentration (mol of NPs/liter) of 10 nm AgNPs standard solutions, the following equation was obtained: $A_{SPR} = 3.83E18 + 0.00806 * C$, with R^2=0.999. Therefore the calculated extinction coefficient for 10 nm AgNPs was: $\varepsilon = 3.83E8\ M^{-1}cm^{-1}$ and the molar concentration of AgNPs used in this work was 2.2 nM.

4.4 Gold Nanoparticles in water

The same procedure described for AgNPs was used to find out the best experimental conditions for producing the AuNPs. First the wavelength and absorbance of the SPR band was monitored as a function of laser ablation time for 20 minutes, then the colloidal solutions produced at different laser ablation times were tracked for 3 weeks to test their stabilities. The laser ablation time chosen for the experiments was 10 min.

Figure 3 reports the SPR spectrum of the AuNPs produced by PLAL and used in this work. As widely illustrated in the literature [20, 21, 22] it is possible to determine the size and the concentration of spherical AuNPs in acqueous solution from SPR absorption spectra. In the references quoted above a wide range of AuNPs (diameter from 3 to 120 nm) have been analysed by using theoretical and experimental approaches. In particular, different approaches are needed for

AuNP having diameters smaller than 25 nm for which the Mie theory is not more valid with respect to those used for NPs having diameter bigger than 25 nm . For instance, in ref. [21], by comparing the theoretical and experimental data, different SPR wavelength dependences on NPs diameters have been found for these two cases. For AuNPs with size smaller than 25 nm (as those produced in this work), there is a logarithmic dependence of the size upon the ratio between the absorbance at the SPR peak (A_{SPR}) and that at 450 nm (A_{450}), that can be used to deduce the AuNPs size.

In the present case to determine the size of AuNPs produced by PLAL, a calibration curve has been performed for obtaining the empirical equations as described in [21]. After the SPR spectra acquisition of standard AuNPs solutions of different sizes at fixed concentration, by plotting the ratio A_{SPR} /A_{450} as function of ln(d), (fitted by the equation: y=0.428x+0.556, with R^2=0.995) the following equation for size determination has been determined:

$$d = \exp\left(\mathbf{2.34}\frac{A_{SPR}}{A_{450}} - \mathbf{1.29}\right) \qquad \textbf{Eq. 1}$$

where *d* is the AuNPs diameter (nm).

Once NPs size has been determined, the calculation of solution concentration can be performed by Lambert Beer law. The determination of the concentration from SPR spectrum requires the previous estimate of the extinction coefficient ε, also dependent upon the NPs size. In the present case ε has been determined for each AuNPs size through the calibration curves of absorbance as function of concentration of AuNPs standard solutions and then a relation between ε and *d* has been found by plotting the logarithm of extinction coefficient as a function of logarithm of the NPs diameter, as reported in ref. [26]. The fitting of the experimental data led to the following equation for the determination of the extinction coefficient as function of NPs size:

$$\ln \varepsilon = 3.18 \ \ln d + 11.22 \qquad \textbf{Eq. 2}$$

where *d* is the AuNPs diameter (nm) and ε is the extinction coefficient ($M^{-1}cm^{-1}$). The coefficients of eqs. 1 and 2 are in good agreements with those reported by other authors ([21] and [26]).

The size of AuNPs and the extinction coefficient, calculated from eqs. 1 and 2, are d = 15 ± 4 nm and $\varepsilon = 4.1E8\ M^{-1}cm^{-1}$, respectively, and the molar concentration is 2.4 nM.

5. **Interaction of Silver and Gold Nanoparticles with Ubiquitin**

The AgNPs were incubated with Ub and the solutions were monitored as a function of time with SPR spectra

After protein addition, the aggregation of NPs is tracked by analysing the redshift shoulder appearing on the main SPR band. As shown in Figure 4a, soon after the addition of Ub, a red shift by about 5 nm of the SPR band indicates the formation of the protein corona, then a second SPR band appears whose wavelength (λ_{SPR_peak2}) varies with time (Fig.4b) in accord with an increase of the aggregate dimensions. Finally, the wavelength of this second SPR band reaches a critical value corresponding to the maximum size the aggregates can attain before their precipitation occurs. In Figure 5 it is reported the absorbance of the two SPR bands as a function of time: the decrease in absorbance of the first SPR peak indicates that most of the isolated AgNPs contribute to the formation of aggregates, that can be appreciated by the increase in absorbance of the second SPR peak. The aggregation process is rather fast so that 30 min after mixing the two absorbance values remain rather constants, presenting only a slight variation with time. After two days the aggregates start to precipitate. Figure 6 shows TEM images of the aggregates in solution as well as in the precipitate formed after two days. The micrographs confirm the presence of large aggregates also in solution and show that the precipitate consists of large protein deposits surrounding the NPs. Inspection of the TEM images with negative staining clearly reveals that Ub surrounds completely each AgNP forming the aggregate, indicating that is the protein corona responsible for the NPs aggregation. In this context, it is important to ascertain if during the NPs aggregation Ub undergoes a transformation. In ref. [12] it was shown that while Ub induces the clustering of the naked AgNPs, it undergoes an amyloid transition. Moreover, a specific mutation (Glu16Val at one edge β-strand) appears to be critical.

The interaction between AgNPs and Ub appears to be extremely dependent upon the presence in solution of some stabilizer. In Figure 7, a and b, are shown the absorbance spectra of AgNPs incubated with Ub after addition of sodium citrate or sodium phosphate to the solution. In both cases, there is no formation of aggregates after 24 h incubation. Only in the case of AgNPs stabilized with phosphate, a red shifted shoulder appears at longer incubation times indicating the presence of a small fraction of NP clustering, which remains unchanged even after three weeks.

In Figure 7b, it is possible to note that the the λ_{SPR} of AgNPs+phosphate is 396 nm and that of AgNPs+citrate is 399 nm (Fig. 7a), whereas the λ_{SPR} of the native, naked AgNPs was 398 nm. It is known that the addition of different kinds of ions in a solution of ligand-free NPs leads to a different buffering effect since they transfer their charges to the NP surface altering their electrostatic stabilization. As already reported in the literature, while the citrate is efficiently absorbed on NP (as confirmed by the red shift of λ_{SPR}), the main action of the phosphate is to change the ionic strength of the solution leading not only to a further NPs stabilization but also to a slight size quenching effect as confirmed by the blue shift of the λ_{SPR} and as reported in ref. [27]).

In both cases (Fig. 7, a and b), the NP surface modification is so effective that no NP clustering and no Ub transformation occur, as the AgNPs are coated before their interaction with Ub. In Figure 7c is also shown that, if citrate is added after the interaction between naked AgNPs and Ub is started (in the shown experiment it was added 81 min after addition of the protein), the aggregation process is stopped. By comparing Figures 4a and 7c, it is also evident that without citrate, the aggregates grow so much that they precipitate after two days; in contrast, the addition of citrate, 81 min after mixing NPs and Ub, "freezes" the aggregates, that remain unchanged and do not give any visible precipitate even after six days. Since the aggregates are clusters of NPs surrounded by protein, the citrate probably surrounds the formed clusters, thus preventing their further growth.

When naked AuNPs were incubated with Ub, a behavior similar to that just described for AgNPs was observed. The interaction between AuNPs and Ub was already investigated, but only in the case of coated AuNPs [28, 29]. In that case, only protein corona formation was observed and this was investigated both from a theoretical and an experimental point of view. In the present work, AuNPs, previously coated with citrate as stabilizer, also lead to the formation of an Ub corona (monitored by the typical red shift of the λ_{SPR}). In contrast, when naked AuNPs are treated with Ub, a very fast aggregation process takes place confirmed by a large value of λ_{SPR_peak2} reached few minutes after mixing (Fig. 8, a and b). By inspection of Figure 8b and 9 it is evident that the rate of aggregate formation is very high. By comparing Figure 8b and Figure 4b it is clearly visible that the λ_{SPR_peak2} of AuNPs-Ub (Figure 8b) and AgNPs-Ub system (Figure 4b) employs 2 and 28 minutes, respectively to reach a constant value. Moreover, in Figure 9 it is shown that within the first 4 minutes after the mixing the absorbance of the two SPR peaks has behaviors similar to those observed for the AgNPs and Ubiquitin interaction (Figure 5), but the time at which absorbance of λ_{SPR_peak1} and the absorbance of λ_{SPR_peak2} reach constant values are different. For longer times of Figure 9 (after 4 minutes), both SPR peaks start to decrease indicating the beginning of the precipitation process. 12 h after mixing the aggregate precipitation can be considered as complete, on the contrary the precipitation of the aggregate formed after the AgNPs and Ub mixing was considered complete only after 2 days. The maximum red shift of the λ_{SPR_peak2} with respect to the λ_{SPR} of native NPs ($\Delta\lambda_{SPR} = \lambda_{SPR\_peak2} - \lambda_{SPR}$) for the two complex systems (AgNPs-Ub and AuNPs-Ub), immediately before precipitation, were found to be 80 and 120 nm, respectively. Thus, the dimensions of the aggregates in the AuNPs-Ub system are bigger than those of the AgNPs-Ub system. These results can be possibly a consequence, among other factors, of the larger size (lesser curvature) and surface area of naked AuNPs compared to AgNPs. It is concluded that, in the experimental conditions used in this work, the reactivity of the gold surface towards Ub is greater than that of the silver surface.

Finally, in order to understand if the type of modification that Ub is undergoing is similar for naked AgNPs and AuNPs, some experiments have been performed on AuNPs, before and after the interaction with Ub. It was already demonstrated (ref. [12]) that naked AgNPs promote a remarkable amyloid transition of Ub (Aβ-like aggregation), while the protein induces the clustering of AgNPs. In order to confirm that also AuNPs induce an amyloid transition of Ub, tranthyretin, a well known inhibitor of amyloid-type aggregation of protein, has been added to the AuNPs solution before the treatment with Ub (named [AuNPs+TTR]+Ub solution). By monitoring with SPR spectra of the solution for 24 h, it was evident that no AuNPs clustering occurs (Fig10a) and it can be assumed that Ub does not have any amyloid transition because TTR inhibits the amyloid-like aggregation. As a further test to confirm that when the Ub amyloid transition is blocked also the AuNPs clustering is prevented, the incubation of AuNPs with a Ub mutant has been performed and monitored in time (the solution was named AuNPs+E16V) with SPR spectra. The Ub mutant used here is E16V that lacks of a negatively charge residue (a Glu16 was replaced by a Val) because this specific mutation site of Ub appears to be critical [12] during the interaction with naked NPs. As in the case of the incubation of AgNPs with E16V, also in this case no AuNPs aggregation was observed at long time after the solution preparation (Fig. 10a). In this frame Glu16 of Ub plays a key role for promoting AuNPs aggregation since it is required for the amyloid transition. Finally, to confirm the presence of amyloid-like structure in the AuNPs-Ub aggregates, ThT fluorescence assays have been performed on Ub solution, on AuNPs solution, on [AuNPs+TTR]+Ub solution and on the the AuNPs-Ub aggregate after the incubation of AuNPs with Ub. When thyoflavin bind an amyloid structure it acts as dye and an intense fluorescence can be detected by acquiring images with the confocal microscope. The Ub, AuNPs and [AuNPs+TTR]+Ub solutions treated with ThT did not exhibit any positive response, while AuNPs-Ub aggregate gave an intense fluorescence, as it can be observed in Fig10b, confirming that Ub of AuNPs-Ub aggregate undergoes to an amyloid transition. In conclusion, besides the naked AgNPs, also naked AuNPs promotes an amyloid-like transition of Ub. Therefore, even if the surface reactivity of naked AuNPs toward Ub is greater than that of naked AgNPs, the changes induced in the protein are substantially the same.

Conclusions

In this work AgNPs and AuNPs were produced by PLAL in order to obtain naked NPs without any undesired contaminant or stabilizer. After the optimization of the experimental conditions for obtaining a good reproducibility of particle size, concentration, and stability of NPs, the interaction with Ubiquitin was studied. Unlike the wet-chemical method usually used for the preparation of metal NPs (which requires the chemical reduction of a metal salt and the use of stabilizers), in this study we used naked NPs produced by PLAL to test how the NPs surface reactivity can change the

processes undergoing to the interaction between NPs and proteins. The surface reactivity of an NP is strongly influenced by the presence of salts or stabilizers in solution, since they act on the resultant NP surface activity.

Initially, we tested the interaction of Ub with citrate-coated AgNPs and AuNPs confirming the typical protein corona formation. Then the naked AgNPs and AuNPs were incubated with Ubiquitin: after initial formation of a protein corona, the systems evolve into clusters of NP followed by the precipitation of formed aggregates after a certain time. At the experimental conditions used in this work, the reactivity of AuNPs surface results higher than the corresponding one of the AgNPs. The results show that the Ubiquitin induces the clustering of the NPs in large aggregates and simultaneously the protein itself undergoes to an amyloid transition. Since Ub is usually a stable protein of human with a compact fold, which does not have tendency to aggregate, the comprehension of the destabilization mechanisms of Ub when interacts with NPs can be a key issue in addressing the problem of nanotoxicity in different biological or medical applications.

Acknowledgments

The authors thank prof. Gerardo Palazzo (Department of Chemistry, University of Bari "Aldo Moro") and the Italian Ministry for Education, University and Research (PON Project "Laboratorio per lo Sviluppo Integrato delle Scienze e delle Tecnologie dei Materiali Avanzati e per dispositivi innovativi - LABORATORIO SISTEMA") for the fluorescence microscopy measurements.

References

1. C. Rehbock, J. Jakobi, L. Gamrad, S. van der Meer1, D. Tiedemann, U. Taylor, W. Kues, D. Rath, S. Barcikowski, Current state of laser synthesis of metal and alloy nanoparticles as ligand-free reference materials for nano-toxicological assays, J. Nanotechnol. (2014), *5*, 1523–1541.
2. V. Amendola and M. Meneghetti, What controls the composition and the structure of nanomaterials generated by laser ablation in liquid solution?, Phys.Chem. Chem. Phys., (2013), 15, 3027
3. M. Dell'Aglio , R. Gaudiuso , O. De Pascale , and A. De Giacomo , " Mechanisms and processes of pulsed laser ablation in liquids during nanoparticle production," Applied Surface Science 348 (2015) 4–9

4. Tamura, A. Matsumoto, K. Fukami, N. Nishi, T. Sakka, Simultaneous observation of nascent plasma and bubble induced by laser ablation in water with various pulse durations, Journal of Applied Physics 117, (2015)173304
5. L. Calzolai, S. Laera, G. Ceccone, F. Rossi, Structure and Stability of Proteins Interacting with Nanoparticles, Chap. 3 In Proteins at Interfaces III State of the Art; Horbett, T., et al.;ACS Symposium Series; American Chemical Society: Washington, DC, 2012.
6. E. Casals, T. Pfaller, A. Duschl, G. J. Oostingh, V. F. Puntes, Hardening of the Nanoparticle–Protein Corona in Metal (Au, Ag) and Oxide (Fe3O4 , CoO, and CeO2) Nanoparticles, Small (2011) 7, No. 24, 3479–3486
7. S. R. Saptarshi, A. Duschl, A. L Lopata, Interaction of nanoparticles with proteins: relation to bio-reactivity of the nanoparticle, Journa of Nanobiotechnology (2013), 11:26
8. S. Grade, J. Eberhard, A. Neumeister, P. Wagener, A. Winkel, M. Stiesch, S. Barcikowski, Serum albumin reduces the antibacterial and cytotoxic effects of hydrogelembedded colloidal silver nanoparticles, RSC Advances, (2012), 2, 7190–7196
9. Rehbock, V. Merk, L. Gamrad, R. Streubel, S. Barcikowski, Size control of laser-fabricated surfactant-free gold nanoparticles with highly diluted electrolytes and their subsequent bioconjugation, Phys. Chem. Chem. Phys., (2013), 15, 3057
10. V. Amendola, M. Meneghetti, Controlled size manipulation of free gold nanoparticles by laser irradiation and their facile bioconjugation, J. Mater. Chem., 2007, 17, 4705–4710.
11. R. Podila, R. Chen, P. C. Ke,J. M. Brown, A. M. Rao, Effects of surface functional groups on the formation of nanoparticle-protein corona, Applied Physics Letters 101, (2012) 263701
12. V. Mangini, M. Dell'Aglio, A. De Stradis, A. De Giacomo, O. De Pascale, G. Natile, F. Arnesano, Amyloid transition of ubiquitin on silver nanoparticles produced by pulsed laser ablation in liquid as a function of stabilizer and single-point mutations, Chem. Eur. J. (2014), 20, 10745 – 10751
13. F. Ding, S. Radic, R. Chen, P. Chen, N. K. Geitner, J. M. Brown, P. C. Ke. Nanoscale. Direct observation of a single nanoparticle-ubiquitin corona formation, (2013), 5(19), 9162-9169.
14. M. Dell'Aglio, R. Gaudiuso, R. ElRashedy, O. De Pascale, G. Palazzo, A. De Giacomo, Collinear double pulse laser ablation in water for the production of silver nanoparticles, Phys.Chem. Chem. Phys., (2013), 15, 20868
15. De Giacomo, M. Dell'Aglio, A. Santagata, R. Gaudiuso, O.De Pascale, P. Wagener, G. C. Messina, G. Compagnini and S.Barcikowski, Cavitation dynamics of laser ablation of bulk and wire-shaped metals in water during nanoparticles production, Phys.Chem. Chem. Phys., (2013),15, 3083

16. H. Muto, K. Yamada, K. Miyajima, F. Mafune´, Estimation of Surface Oxide on Surfactant-Free Gold Nanoparticles Laser-Ablated in Water, J. Phys. Chem. C (2007), 111, 17221-17226
17. V. Merk, C. Rehbock, F. Becker, U. Hagemann, H. Nienhaus, S. Barcikowski, In Situ Non-DLVO Stabilization of Surfactant-Free, Plasmonic Gold Nanoparticles: Effect of Hofmeister's Anions, Langmuir (2014), 30, 4213−4222
18. J. A. Creighton, D. G. Eadon, Ultraviolet–visible absorption spectra of the colloidal metallic elements, J. Chem. Soc., Faraday Trans., (1991),87, 3881-3891
19. V. Amendola, O. M. Bakr, F. Stellacci, A Study of the Surface Plasmon Resonance of Silver Nanoparticles by the Discrete Dipole Approximation Method: Effect of Shape, Size, Structure, and Assembly, Plasmonics (2010) 5:85,–97
20. W. Jacak, J. Krasnyj, J. Jacak, R. Gonczarek, A. Chepok, L. Jacak, D. Z. Hu, D. Schaadt, Radius dependent shift of surface plasmon frequency in large metallic nanospheres: theory and experiment, Journal of Applied Physics, (2010); 107(12):124317 - 124317-13.
21. W. Haiss, N.T. K. Thanh, J. Aveyard, and D. G. Fernig, Determination of Size and Concentration of Gold Nanoparticles from UV-Vis Spectra, Anal. Chem. (2007), 79, 4215-4221.
22. D. Evanoff, Jr., G. Chumanov, Size-controlled synthesis of nanoparticles. 2. Measurement of extinction, scattering, and absorption cross sections, J. Phys. Chem. B, (2004), 108, 13957-13962
23. L. Gonzàlez, C. Noguez, G. P. Ortiz, G. Rodrìguez-Gattorno, Optical Absorbance of Colloidal Suspensions of Silver Polyhedral Nanoparticles, J. Phys. Chem. B (2005), 109, 17512-17517
24. Yang, Laser Ablation in Liquids: Principles and Applications in the Preparation of Nanomaterials, Published: February 22, 2012 by Pan Stanford
25. H. Ohshima, The Derjaguin – Landau –Verwey – Overbeek (DLVO), Theory Of Colloid Stability, Chapter 3 in Electrical Phenomena at Interfaces and Biointerfaces: Fundamentals and Applications in Nano-, Bio-, and Environmental Sciences, First Edition. Edited by Hiroyuki Ohshima. © 2012 John Wiley & Sons, Inc.
26. X. Liu, M. Atwater, J. Wang, Q. Huo, Extinction coefficient of gold nanoparticles with different sizes and different capping ligands, Colloids and Surfaces B: Biointerfaces 58 (2007) 3–7G.
27. Pfeiffer, C. Rehbock, D. Huhn, C. Carrillo-Carrion, D. Jimenez de Aberasturi, V. Merk,S. Barcikowski, W. J. Parak, Interaction of colloidal nanoparticles with their local environment:

the (ionic) nanoenvironment around nanoparticles is different from bulk and determines the physico-chemical properties of the nanoparticles,2013, J. R. Soc. Interface 11:20130931.

28. F. Tavanti, A. Pedone, M. C. Menziani, A closer look into the ubiquitin corona on gold nanoparticles by computational studies, New J. Chem., (2015), 39, 2474

29. G. Brancolini, D. B. Kokh, L. Calzolai, R. C. Wade, S. Corni. Docking of Ubiquitin to Gold Nanoparticles, ACS Nano (2012), 6(11), 9863-9878.

Figure captions

Fig. 1. λ_{SPR}, absorbance and FWHM of the SPR band of AgNPs as a function time after laser ablation.

Fig. 2. SPR spectrum of AgNPs colloidal solution. In the inset, a TEM micrograph of AgNPs is shown. The determined size is indicated.

Fig. 3. SPR spectrum of AuNPs colloidal solution. The calculated size, extinction coefficient, and molar concentrations are indicated.

Fig. 4. Temporal evolution of the SPR spectrum a) and λ_{SPR_peak2} (relative to the second SPR band) b) after incubation of naked AgNPs with Ubiquitin.

Fig. 5. Temporal evolution of the absorbance of two SPR bands , λ_{SPR_peak1} and λ_{SPR_peak2}, after incubation of naked AgNPs with Ubiquitin.

Fig. 6. TEM micrographs of the AgNPs-Ubiquitin system without a) and with b) negative staining, taken after 24 h incubation of Ubiquitin with naked AgNPs, and c) TEM micrograph with negative staining of the precipitate formed after 48h incubation.

Fig. 7. SPR spectra of a) AgNPs after addition of citrate and further incubation of "AgNPs+citrate" with Ubiquitin; b) AgNPs after addition of phosphate and further incubation of "AgNPs+phosphate" with Ubiquitin. c) SPR spectra of naked AgNPs incubated with Ubiquitin, stopped 81 min after mixing, and then treated with citrate. All the solutions were monitored at different times after mixing.

Fig. 8. Temporal evolution of the SPR spectrum a) and λ_{SPR_peak2} (relative to the second SPR band) b) after incubation of naked AuNPs with Ubiquitin.

Fig. 9. Temporal evolution of the absorbance of two SPR bands , λ_{SPR_peak1} and λ_{SPR_peak2}, after the incubation of naked AuNPs with Ubiquitin.

Fig. 10. a) Comparison of SPR spectra of AuNPs alone, AuNPs with Ub after 85 min incubation (AuNPs+Ub), AuNPs preincubated with TTR (3 μM) and then treated with Ub after 24 h incubation ([AuNPs+TTR]+Ub), AuNPs with the Ub mutant E16V after 24 h incubation (AuNPs+E16V). b) Fluorescence microscopy image of AuNPs-Ub aggregates stained with ThT. The boxed area is enlarged in the inset to show the presence of fibrillar structures of Ub molecules that underwent an amyloid transition.

Figures

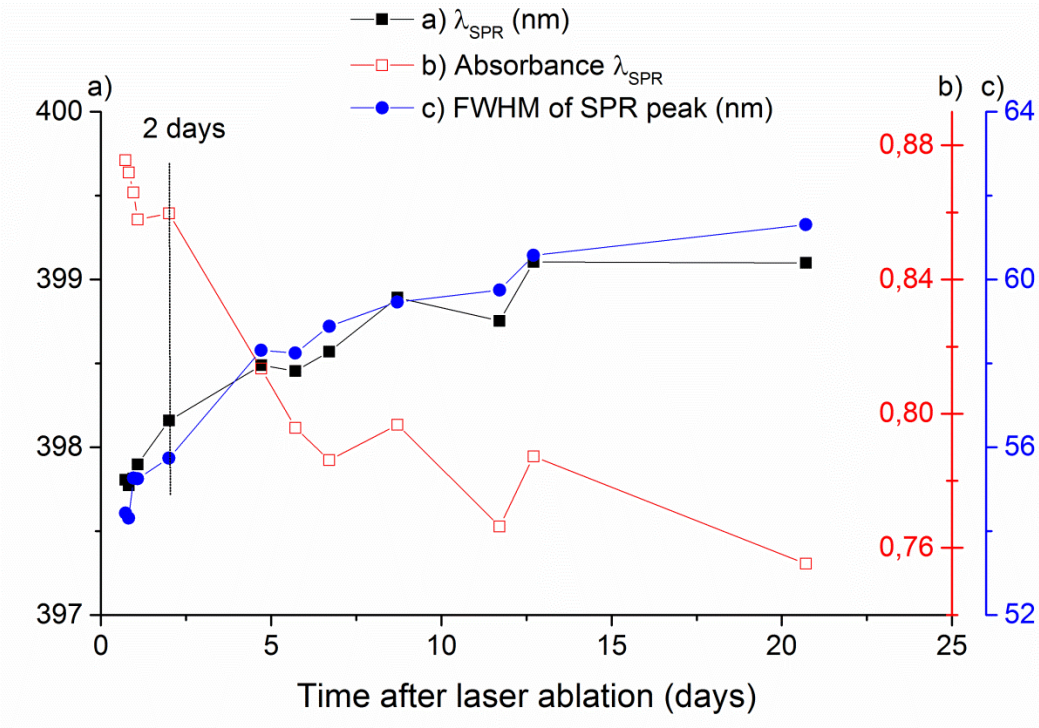

Figure 1

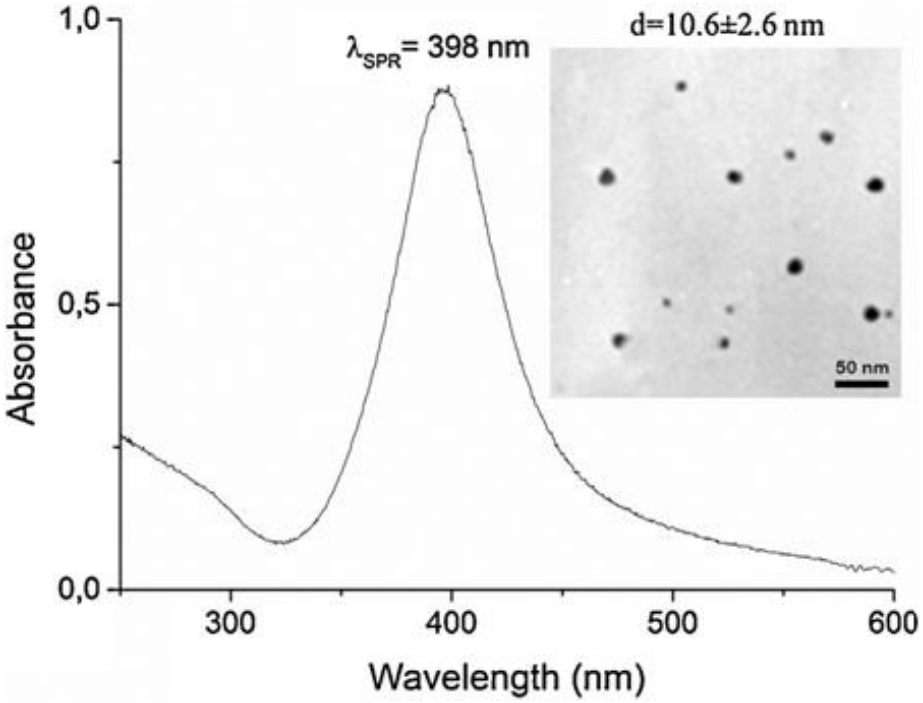

Figure 2

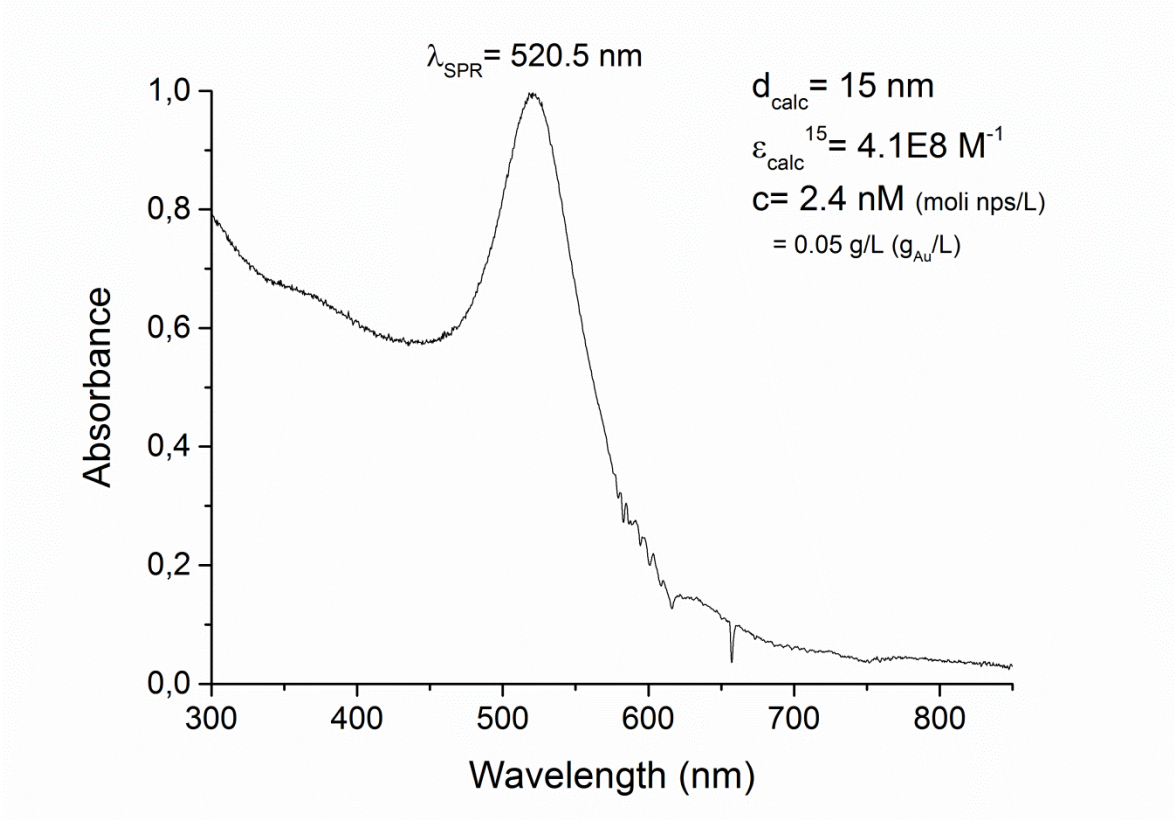

Figure 3

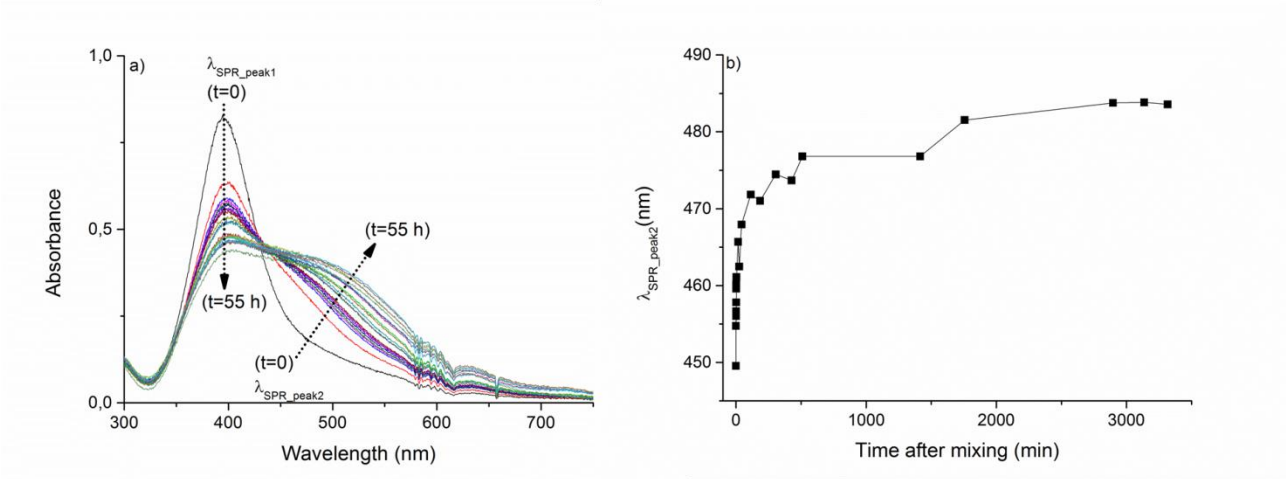

Figure 4

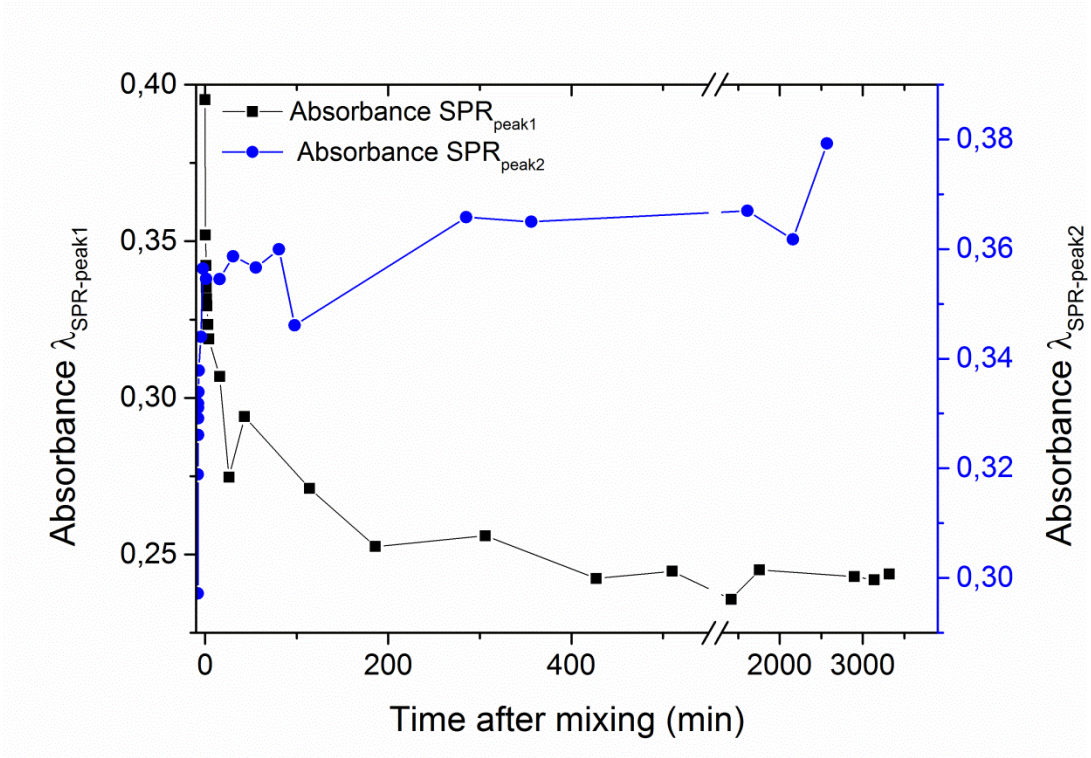

Figure 5

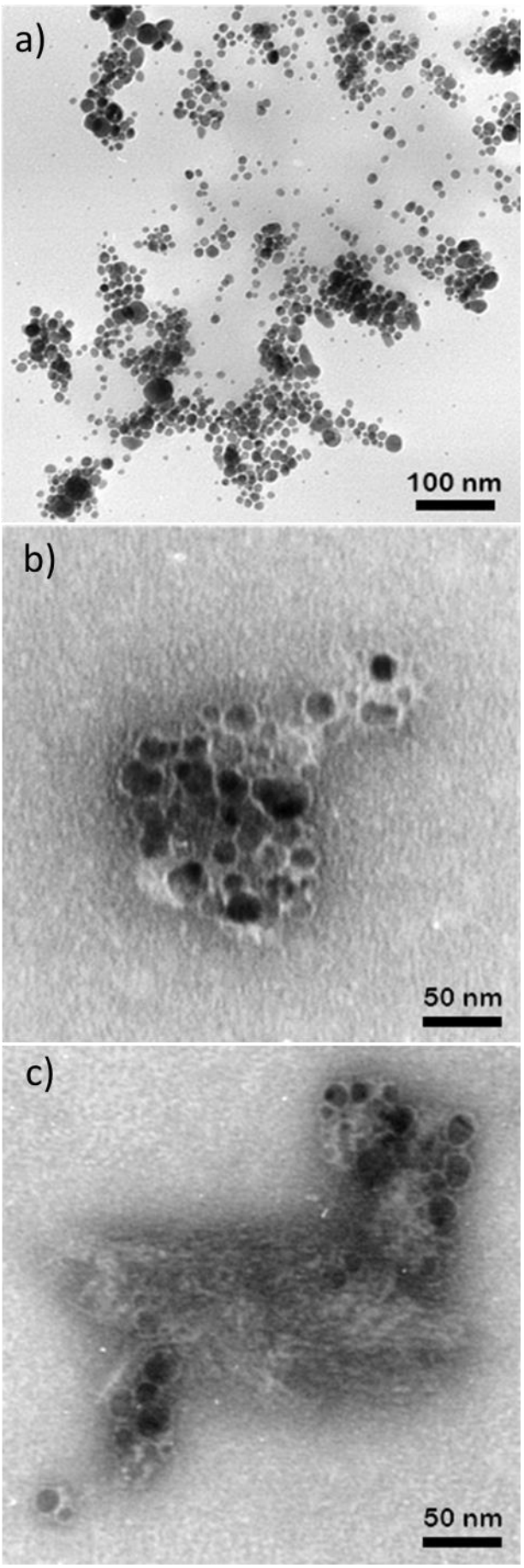

Figure 6

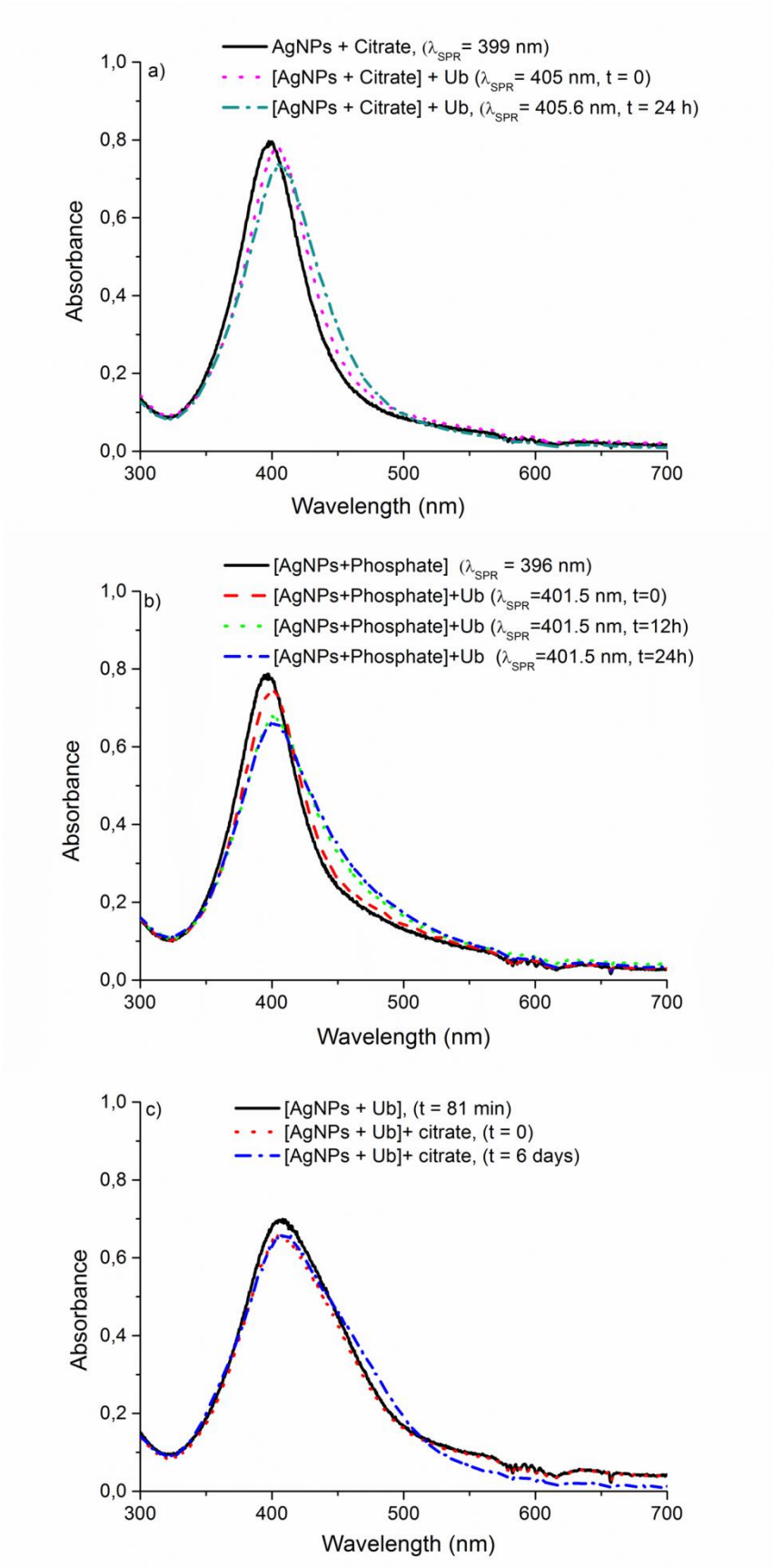
a)
AgNPs + Citrate, (λSPR= 399 nm)
[AgNPs + Citrate] + Ub (λSPR= 405 nm, t = 0)
[AgNPs + Citrate] + Ub, (λSPR= 405.6 nm, t = 24 h)
Absorbance
Wavelength (nm)
b)
[AgNPs+Phosphate] (λSPR = 396 nm)
[AgNPs+Phosphate]+Ub (λSPR=401.5 nm, t=0)
[AgNPs+Phosphate]+Ub (λSPR=401.5 nm, t=12h)
[AgNPs+Phosphate]+Ub (λSPR=401.5 nm, t=24h)
Absorbance
Wavelength (nm)
c)
[AgNPs + Ub], (t = 81 min)
[AgNPs + Ub]+ citrate, (t = 0)
[AgNPs + Ub]+ citrate, (t = 6 days)
Absorbance
Wavelength (nm)

Figure 7

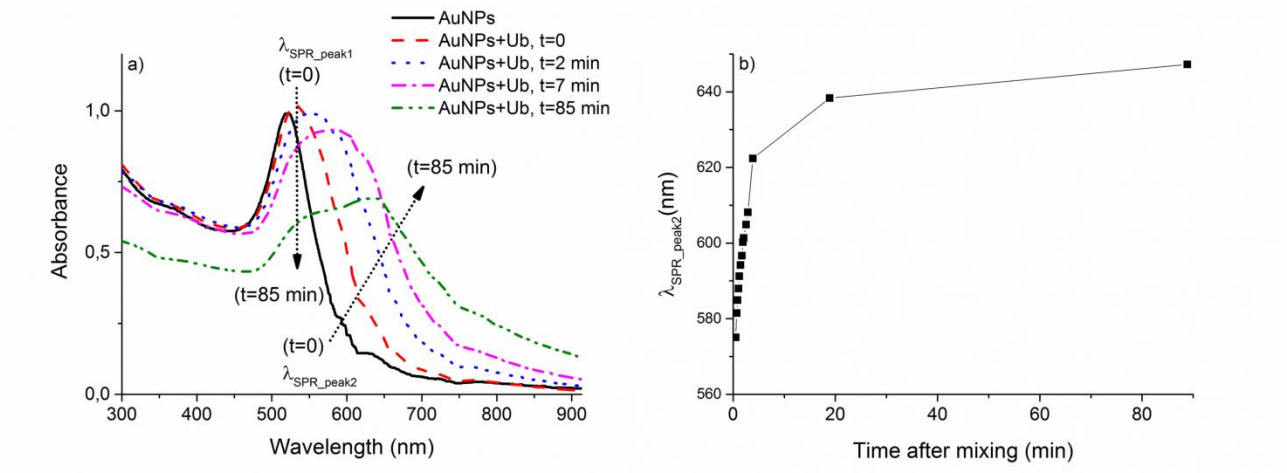

Figure 8

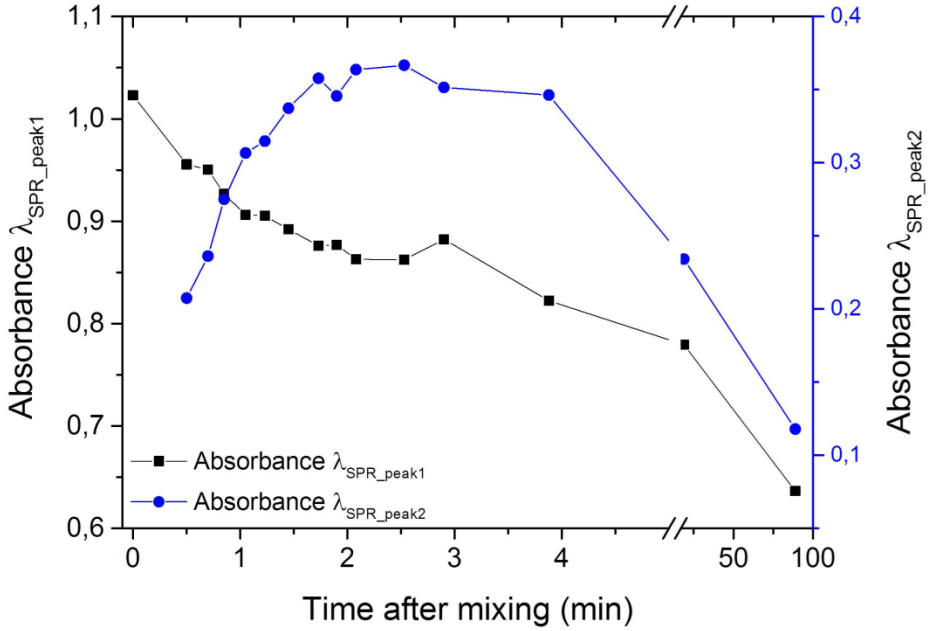

Figure 9

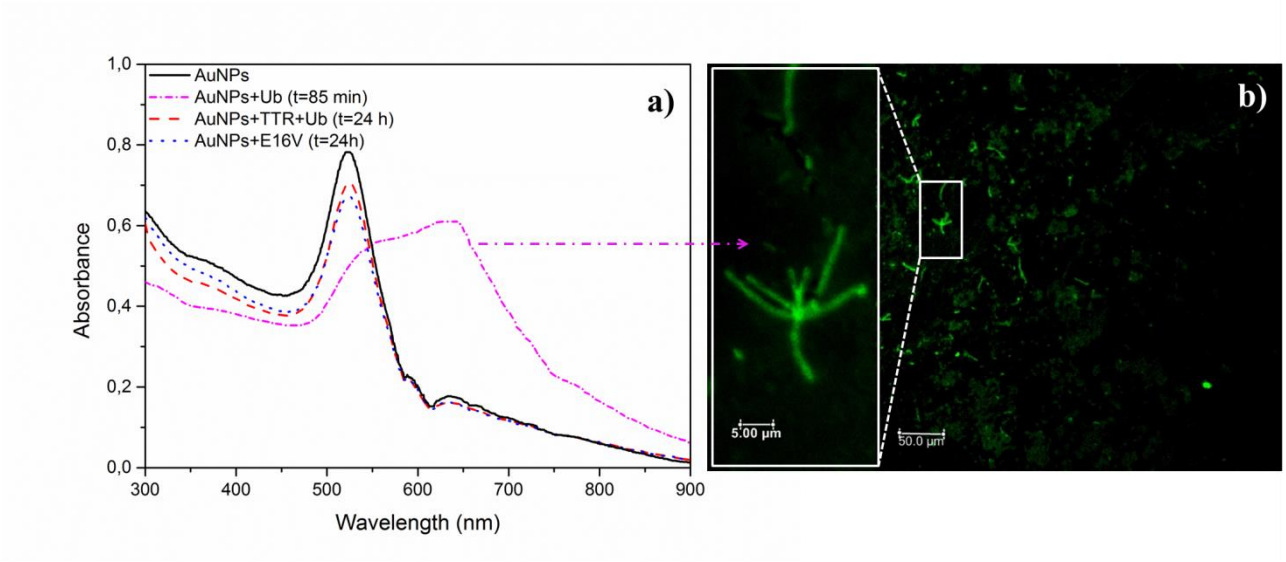
AuNPs
AuNPs+Ub (t=85 min)
AuNPs+TTR+Ub (t=24 h)
AuNPs+E16V (t=24h)
a)
b)
Absorbance
Wavelength (nm)
1,0
0,8
0,6
0,4
0,2
0,0
300
400
500
600
700
800
900
5.00 µm
50.0 µm

Figure 10